

LIDAR OBSERVATIONS OF THE ANTARCTIC STRATOSPHERIC AEROSOLS

Yasunobu IWASAKA¹, Hiroshi FUKUNISHI², Ryoichi FUJII²,
Hiroshi MIYAOKA² and Takeo HIRASAWA²

¹*Water Research Institute, Nagoya University, Furo-cho, Chikusa-ku, Nagoya 464*

²*National Institute of Polar Research, 9-10, Kaga 1-chome, Itabashi-ku, Tokyo 173*

Abstract: The outline of lidar measurements which were made at Syowa Station (69°00'S, 39°35'E), Antarctica since March 1983 is described. Interesting topic was the enhancement of the stratospheric aerosol layer in winter. Coordinate measurements by the lidar and balloons were successfully done to clarify the early stage of the winter enhancement of the stratospheric aerosol layer.

1. Introduction

The lidar measurements on the stratospheric aerosols have been made at Syowa Station (69°00'S, 39°35'E), Antarctica since March 1983 as part of the international project, Antarctic Middle Atmosphere (AMA). Now a lidar is one of the most powerful instruments to remotely monitor the upper atmosphere. About thirty lidars are located worldwide for monitoring the stratospheric aerosol content and other properties. Unfortunately, most of these lidars are located in the middle latitudinal region of the northern hemisphere, and this has made it very difficult to study the behavior of stratospheric aerosols on a global scale.

The polar stratosphere has been thought to be an active sink region of the stratospheric minor gases and particulate matter, but this idea has not been verified theoretically and observationally. Additionally, the polar middle atmosphere is an interesting and attractive region from the viewpoint of atmospheric aerosol science since there are many atmospheric events which cannot be found in the middle and/or low latitudes. Especially, the active precipitation of high-energy-charged molecules and atoms, the extremely cold stratosphere, and the very cold summer mesopause are typical examples.

This paper gives an outline of the lidar measurements at Syowa Station, Antarctica in 1983.

In winter we observed the extremely enhanced aerosol layer. This event should be essentially the same event as the "Polar Stratospheric Clouds" event measured by satellite (McCORMICK *et al.*, 1982). The balloon measurement which was cooperatively done in early winter to clarify the early stage of the enhancement of the layer suggested a noticeable increase in the number concentration of large particles (MORITA *et al.*, 1984).

2. Lidar System

The lidar equipment used here consists of a transmitter (ruby laser with Galilean telescope) and a receiver (Cassegrain telescope with detection optics), both mounted on an optical bench with detection and analog signal processing electronics. The transmitter-receiver mount, laser power supply, laser cooler and signal processor are supposed to be located in a compartment. When brought to Syowa Station the equipment is subject to restrictions on dimensions and weight, so the system is made in sections to facilitate easy disassembling and reassembling, and is so structured as to permit installation of additional functions or modification of the measuring system. The performance of the lidar system is given in Table 1.

2.1. Laser section

Figure 1 is a block diagram of the transmitter. The performance of the laser used is given in Table 2. Leaked laser beams from the total reflection mirror of a laser cavity are fed directly to the signal processing section or through optical fibers

Table 1. Main characteristics of the laser radar system.

Transmitter			
Laser output		694 nm > 1 J/pulse 347 nm > 0.3 J/pulse	
Laser pulse width		40 ns	
Repetition rate		60 ppm (max.)	
Laser beam divergence		1.6 mrad	
Transmitter optics		Galilean telescope × 4	
Transmitter beam divergence		0.5 mrad (30 mm dia)	
Receiver			
Receiver optics		Cassegrain telescope	
Receiver diameter		500 mm	
F number		F/4.0	
Receiver field of view		0.5–2.0 mrad	
Transmitter/receiver mount			
Vertical direction only (fixed type)			
Detection system			
3-channel detection (typical configuration)			
A-channel	PMT	R-943-02	347 nm + 1.3 nm (P.C.)
B-channel	PMT	R-943-02	694 nm + 0.5 nm (P.C.)
C-channel	PMT	R-1333	694 nm + 0.5 nm (analog)
	PMT	R-1332	347 nm + 1.3 nm (analog)
Signal processing			
Analog method			
A-D converter (ADC)		8-bit resolution Sampling speed 50 ns (max.)	
Photon counting method			
Multichannel counter (MMC)		8-bit counter Range resolution 100 m (min.)	
Data processing			
CAMAC data logging system with minicomputer (MELCOM 70)			

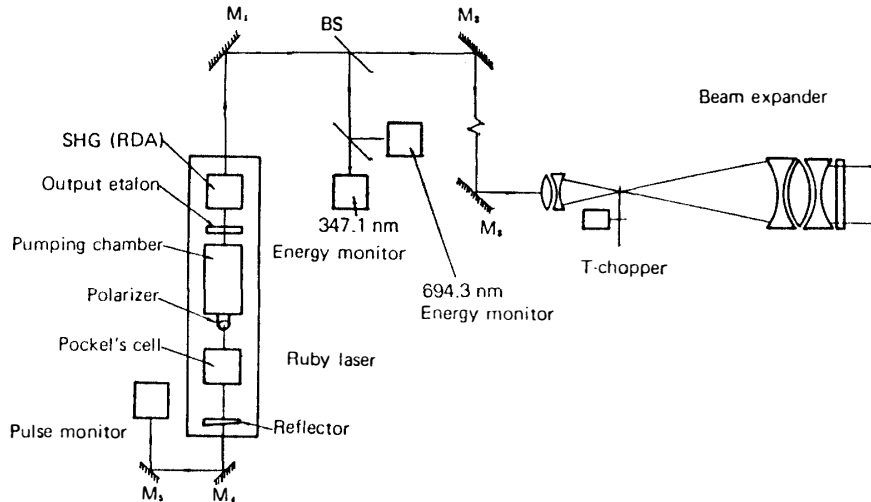


Fig. 1. Schematic picture of the transmitter.

Table 2. Performance of laser.

Laser crystal	Ruby (rod size: $3/8 \times 4$ inches)
Laser output	Primary wave (694 nm) > 1 J/pulse Second harmonic wave (347 nm) > 0.3 J/pulse
Repetition rate	60 ppm (max.)
Cavity length	800 mm
Pulse width	40 ns
Beam divergency	1.6 mrad
Flash lamp	Straight-tube type (4 required)
SHG crystal	RDA (Type 1)
SHG efficiency	25% or more

and are detected by the photodiode to use the trigger signal for the entire system. The He-Ne laser beams for optical axis adjustment are routed similarly.

In order to monitor the laser output for each shot, a part (3%) of the output light is extracted by the partial mirror. The light is separated into two fluxes by a dichroic mirror for detection by the photodiodes. The integration values in the period of 100 ns of the laser waveform (Gated Integrator GAD) are used as energy monitor values. Laser oscillation jitter is 50 ns or less.

2.2. Transmitter optical system

The divergence of laser beams is narrowed to about 0.5 mrad by the transmission telescope via two multiwavelength hard-coated total reflection mirrors and the beams are emitted to the atmosphere. The transmitter telescope is the two-wavelength compensated lens system formed of five lenses in two groups. Focusing is performed to ensure the complete operation of the transmitter chopper. The foresight of the transmitter and receiver optical system is accomplished by adjusting the transmitter telescope to the two axes.

2.3. Receiver optical system

Figure 2 is a block diagram of the receiver. The specifications of the receiver telescope are given in Table 3. This telescope is Cassegrain type and has a dustproof

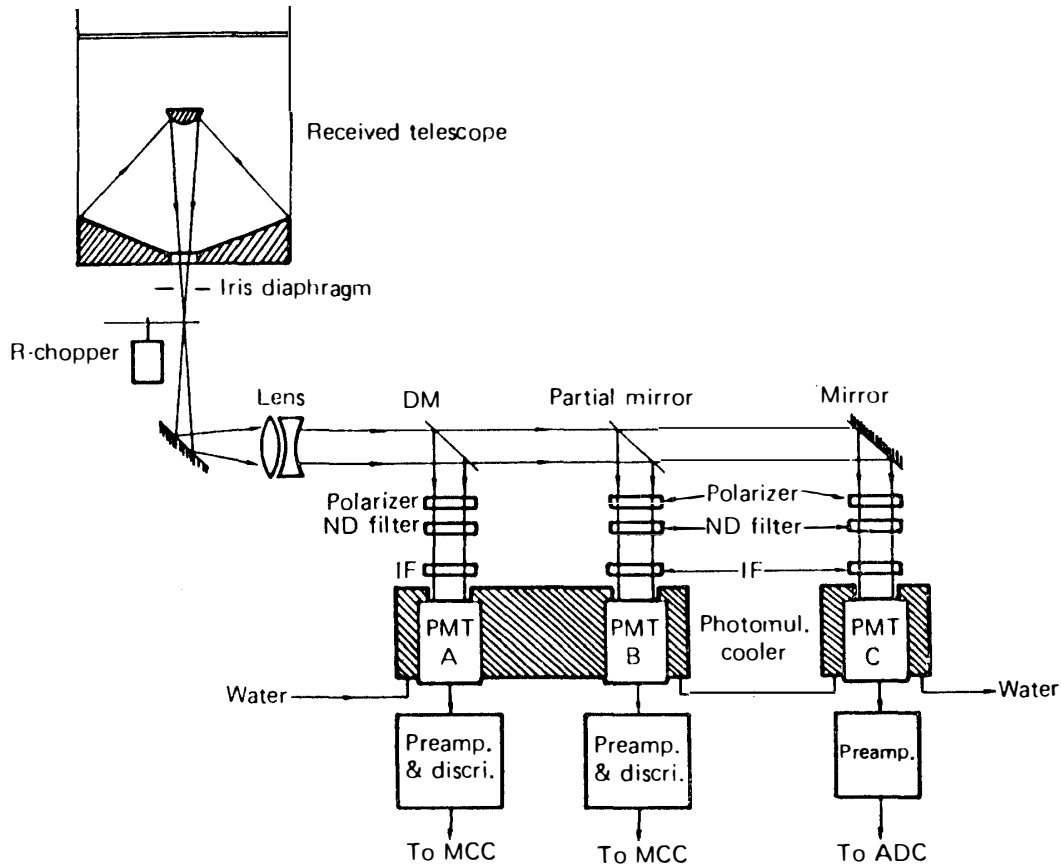


Fig. 2. Schematic picture of the receiver.

Table 3. Performance of receiver telescope.

Reception diameter	500 mm
Focal length	2000 mm
Circle of least confusion	0.25 mm

glass window on the front. A field-of-view iris is provided to vary the field-of-view between 0.5 and 2.0 mrad.

2.4. Detection system

The light flux collected by the receiver telescope is collimated, and divided into three parts by the dichroic mirror, partial mirror, and total reflection mirror. And each flux is fed into three different photomultipliers to perform simultaneously three channel measurements. Two channels (A and B) are used with the photoncounting method, and one channel (C) with the analog method. Channels A and B are used mainly for multiwavelength measurements (694 and 347 nm). All of three channels can be used also with the photoncounting method. Three filters can be set in each channel. An interference filter, ND filter and polarization plate are normally provided in that order. The combination of three mirrors and ND filters can make it possible to cover a wide dynamic range. The photomultiplier tubes are electrically cooled to -20°C to eliminate the effect of the dark current.

A block diagram of the 3-channel photoncounting system also is provided in

Fig. 2. The discriminator, which is using a high-speed computer to compare the photon pulse height to a reference level, generates a 12 ns negative pulse (shaped by the ECL flip-flop) when the input pulse height is above the reference level. Measurements can be continuously made in the three channels with a minimum distance resolution of 100 m, by switching dual three 8-bit high-speed counters (periodical pulse up to 120 MHz can be counted) combined with a 24-bit-width buffer memory (FIFO memory). In the case of 100 m resolution, the speed of writing to the buffer memory is 4.45 Mbit/s.

2.5. Signal processing

A block diagram of the signal processing system is shown in Fig. 3. The system is an assembly of CAMAC modules with microprocessor. Most modules are newly designed following the CAMAC standard. Some digital modules are commercially available ready-made modules. All data are handled by the CAMAC function. The collected data are transferred in the block form to the minicomputer (MELCOM 75/10 system) for display and recording.

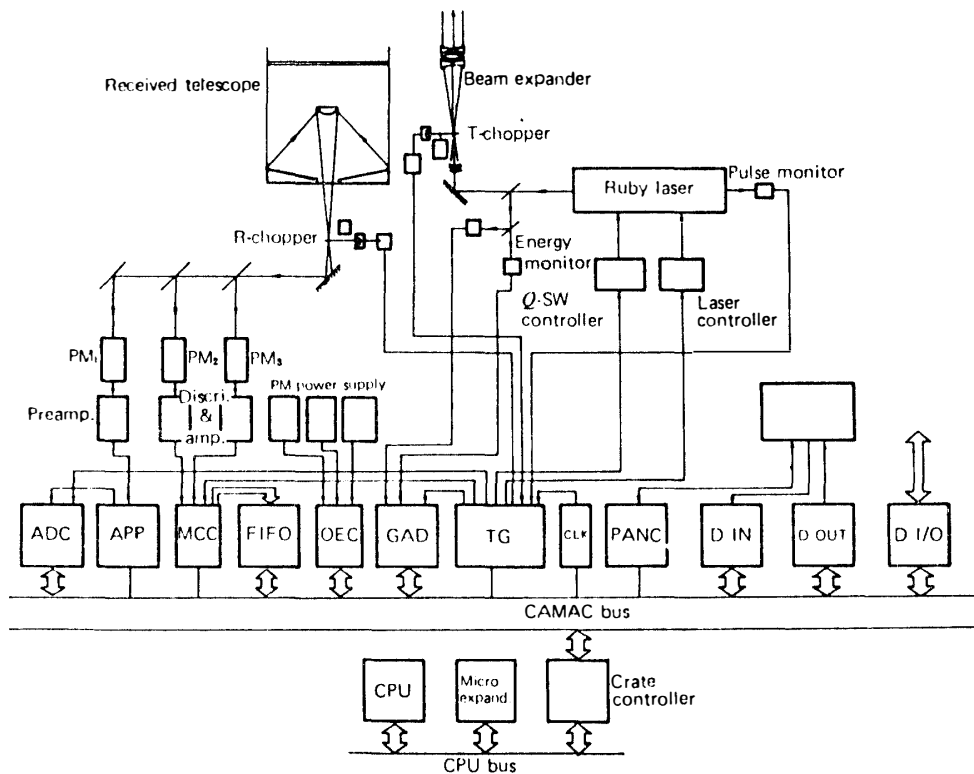


Fig. 3. Block diagram of signal processing unit. ADC: Analog-to-digital converter, APP: Analog preprocessor, MCC: Multichannel counter, FIFO: First-in-first-out memory, OEC: Opto-electro converter, GAD: Gated analog-to-digital converter, TG: Timing generator, CLK: Clock generator, PANC: Panel controller, D IN: Digital input, D OUT: Digital output.

3. Measurement

Lidar measurements were made at Nagoya during the period from June 1982 to

October 1982 to test the system performance. The results showed that the simultaneous multiple wavelength measurement (694 and 347 nm) was a very powerful method of gain information about the nature of scattering source. Details were already described in the previous paper (IWASAKA *et al.*, 1983).

Measurements on the polar stratospheric aerosols have been made at Syowa Station (69°00'S, 39°35'E), Antarctica since March 1983.

During the observational periods, we performed lidar observation under the system condition that the height resolution was 0.5 km, laser pulse power in the range from 0.1 to 0.5 J/pulse, and pulse repetition rate 0.5 Hz.

The scattering ratio is defined by the following relation,

$$R = [B_1 + B_2] / B_1, \quad (1)$$

where B_1 and B_2 are the backscattering coefficients of atmospheric molecules (Rayleigh scattering) and aerosol particles (Mie scattering) respectively. In order to estimate the air molecule scattering we used the measurements of radiosonde which were made at Syowa Station. Additionally the so-called "Matching Method" was used to deduce the backscattering coefficient of aerosol particles (*e.g.*, RUSSEL and HAKE, 1977).

The vertically integrated aerosol scattering (B_2) is given by,

$$\int_{z_2}^{z_1} B_2(z) dz, \quad (2)$$

where z_1 and z_2 are the height of layer top and of layer bottom respectively, and can be recognized as the parameter corresponding the column density of stratospheric particles. When the profile of scattering ratio did not show clearly the layer bottom, we chose the tropopause height instead of the height of layer bottom.

Figure 4 indicates the time change of the vertically integrated backscattering coefficient of aerosols (hereafter we call the vertical integrated backscattering coefficient IBC). Here we should like to give attention to the long-time scale variation in

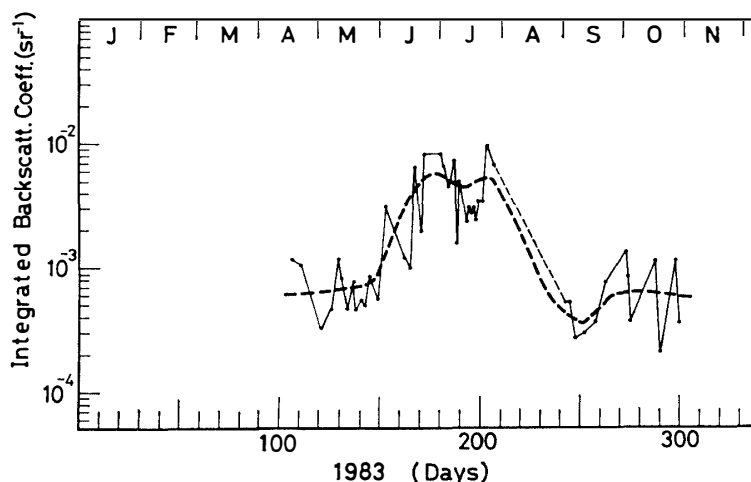


Fig. 4. The vertically integrated backscattering coefficient of aerosols in the Antarctic stratosphere. There is no data during the August of 1983 (dotted line).

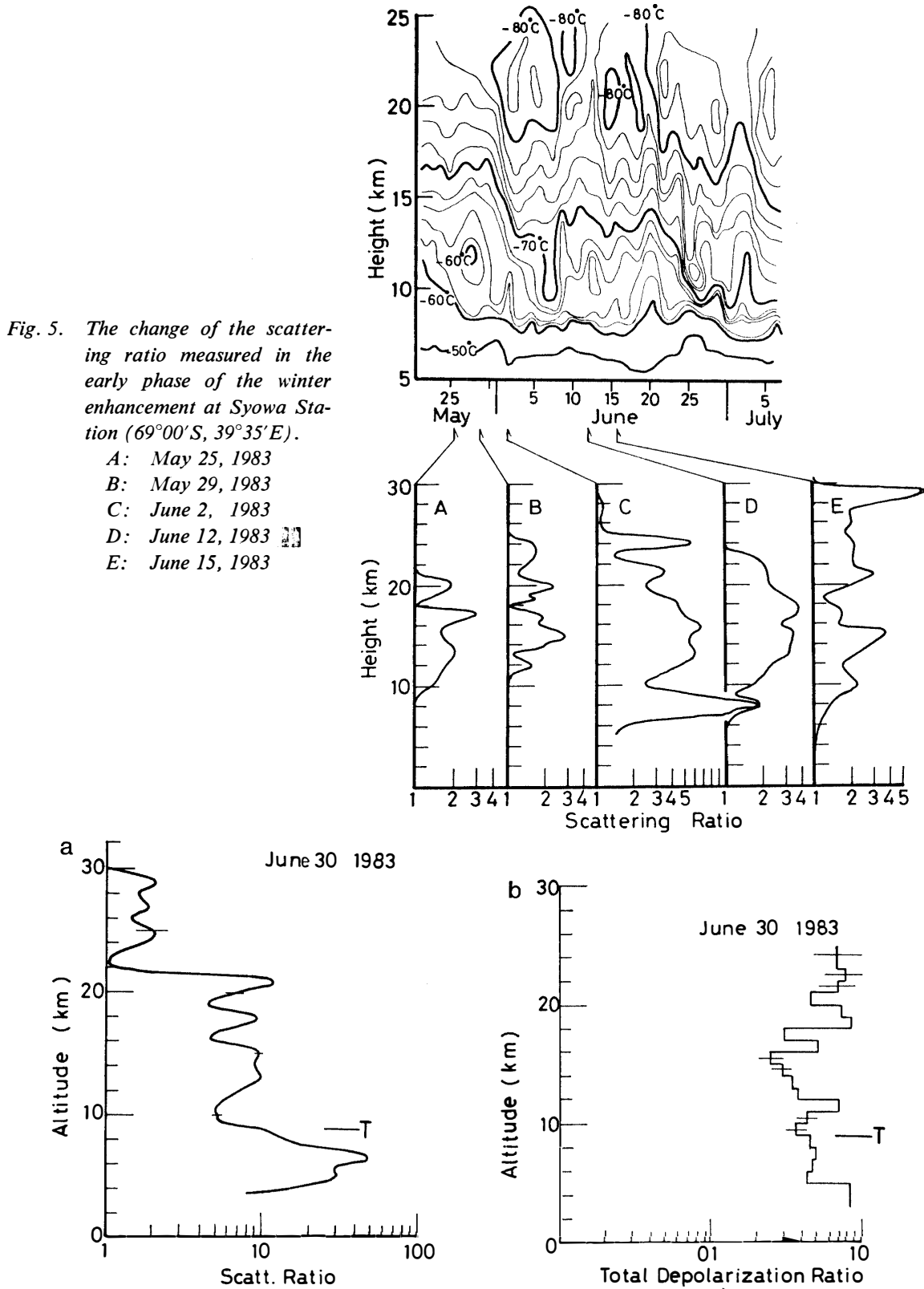


Fig. 5. The change of the scattering ratio measured in the early phase of the winter enhancement at Syowa Station ($69^{\circ}00'S, 39^{\circ}35'E$).

- A: May 25, 1983
- B: May 29, 1983
- C: June 2, 1983
- D: June 12, 1983
- E: June 15, 1983

Fig. 6. The large depolarization ratio measured during the fully developed enhancement of aerosol layer (curve in Fig. 6a shows the profile of scattering ratio and curve in Fig. 6b the profile of depolarization ratio).

the figure. The IBC had its maximum in winter, and this seems to be essentially the same event as the winter increasing ‘‘Polar Stratospheric Cloud’s’’ considering the duration time, the spatial scale, and the intensity of extinction.

The winter enhancement of the stratospheric aerosol layer seems to be strongly correlated to the decrease of the stratospheric temperature in winter. The increase of the scattering ratio, as shown in detail in Fig. 5, was measured in early June 1983 when the temperature dropped below -80°C .

Many cooperative measurements by lidar and balloons were made during the observational periods (MORITA *et al.*, 1984; ITO *et al.*, 1984). Figure 6 shows the typical result, which was gained by the balloon-borne aerosol particle counter on 30 June 1983, indicating the number density of particulate matter in the early phase of the winter enhancement of the stratospheric aerosol layer. Measurements revealed that the noticeable increase of the particle number concentration in the early phase of the enhancement caused the increase of lidar return from the stratosphere.

4. Summary and Discussion

We presented the lidar system used at Syowa Station and some preliminary results of lidar measurements. The measurements suggest that there is a large difference in the nature of the stratospheric aerosols between the high latitudes and mid- and low latitudes. The most important factor which causes such a noticeable difference is certainly the very cold stratospheric condition in the polar winter.

Table 4. Appearance of the enhanced aerosol layer
(Syowa Station, Antarctica, 1983).

	The vertically integrated B_2 was larger than $2 \times 10^{-3}\text{sr}^{-1}$	The vertically integrated B_2 was smaller than $2 \times 10^{-3}\text{sr}^{-1}$
Cold air temperature ($< -80^{\circ}\text{C}$) was measured in the lower stratosphere	36.0%	4.5%
Cold air temperature ($< -80^{\circ}\text{C}$) was not found in the lower stratosphere	0.0%	59.5%

In Table 4 we summarize the occurrence ratio of the enhanced stratospheric aerosol layer on the basis of the lidar measurements in 1983. It can be easily found that the enhanced aerosol layer with the value of IBC larger than $2 \times 10^{-3}\text{sr}^{-1}$ was measured only in the very cold stratosphere with $T < -80^{\circ}\text{C}$. However converses are not always true. Even when the cold air with $T < -80^{\circ}\text{C}$ was found in the lower stratosphere, a few cases did not indicate the enhancement. But such cases are minor ones.

Recently STEELE *et al.* (1983) presented the idea that the active growth of ice crystals was the main process which caused the drastic increase of polar stratospheric particulate matter (and the increase of extinction). According to them the ice crystal growth becomes very active in the cold atmosphere with temperature lower than about -80°C assuming that the water vapor content was about 5 ppmV. If it is so, the polar stratospheric aerosol possibly has influence on various fields; global budget of water vapor, chemistry of sediments in ice sheet, seeding effects on tropospheric clouds,

and so on. This idea should be tested by many observations and theoretical researches. The recent results shown in Table 4 seem to coincide with their idea. Additionally the depolarization ratio of backscattered light from the stratospheric aerosol layer was very high in winter (Fig. 6). Considering that the depolarization ratio of the backscattered light measured at mid-latitude (Nagoya) usually has been in the range from 0.005 (or lower than that) to 0.05 for the quiet there were lots of nonspherical particles in the polar winter stratosphere, and this also supports the ice crystal forming model in the polar stratosphere. Previous studies of the effects of stratospheric particles on light propagation have not paid attention to the presence of nonspherical particles. However, the treatment of nonspherical particles is important for the studies on the particles in the winter polar stratosphere. If we discuss qualitatively the particulate mass concentration and size distribution using only optical technique such as lidar, we face serious difficulties, because the Mie theory describes the light scattered by homogeneous or layered spheres of arbitrary size.

When we estimate the particulate mass from the backscatter coefficients presented here assuming the spherical shape of particles the estimation is probably an underestimated one. It is necessary to gain more precise information about the scattering properties of nonspherical particles in the stratosphere.

Acknowledgments

We should like to thank the wintering members of the 24th Japanese Antarctic Research Expedition (leader Prof. S. MAE, Hokkaido University) for their support of the laser radar measurements. We should like to thank also Assistant General Manager Mr. S. ITOH, Guidance and Electro-Optics Division, EC Corporation, and Mr. M. YASUDA, Guidance and Electro-Optics Division, NEC Corporation, and Mr. H. OHTANI, Guidance and Electro-Optics Division, NEC Corporation for their kind technical supports during the observations.

References

- ITO, T., IKEGAMI, M., KANAZAWA, I. and IWASAKA, Y. (1984): Balloon-borne observation of Aitken nuclei in the Antarctic troposphere and stratosphere. Program and Abstracts; International MAP Symposium, Kyoto, Nov. 26–30, 143.
- IWASAKA, Y., FUKUNISHI, H., HIRASAWA, T., FUJII, R. and MIYAOKA, H. (1983): Simultaneous multiple wavelength laser radar measurement of the stratospheric aerosol layer. *J. Meteorol. Soc. Jpn.*, **61**, 469–472.
- MCCORMICK, M. P., STEELE, H. M., HAMILL, P., CHU, W. P. and SWISSLER, T. J. (1982): Polar stratospheric cloud sightings by SAM II. *J. Atmos. Sci.*, **39**, 1387–1397.
- MORITA, Y., TAKAGI, M., IWASAKA, Y. and ONO, A. (1984): Balloon measurements of aerosols in the Antarctic stratosphere. Program and Abstracts; International MAP Symposium, Kyoto, Nov. 26–30, 142.
- RUSSELL, P. B. and HAKE, R. D., Jr. (1977): The post-Fuego stratospheric aerosol; Lidar measurements, with radiative and thermal implications. *J. Atmos. Sci.*, **34**, 163–177.
- STEELE, H. M., HAMILL, P., MCCORMICK, M. P. and SWISSLER, T. J. (1983): The formation of polar stratospheric clouds. *J. Atmos. Sci.*, **40**, 2005–2067.

(Received April 12, 1985; Revised manuscript received September 17, 1985)